Journal of Power Sources, 39 (1992) 215–224

Diffusional limitations at the lithium polymer electrolyte interface

C. G. Thurston and J. R. Owen*
Chemistry Department, University of Southampton, Highfield, Southampton SO9 5NH (UK)

N. J. Hargreaves
Chemistry Department, University of Salford, The Crescent, Salford M5 4WT (UK)

(Received November 28, 1991; in revised form March 12, 1992)

Abstract

An *in situ* method of monitoring the performance of the cell components was developed to study the capacity losses in solid state rechargeable lithium batteries. A lithium reference electrode was plated onto a fine nickel wire place between two layers of electrolyte in the cell. This technique allowed the deconvolution of the cell potential into both positive and negative cell components. The most significant cause of low capacity was found to be ion starvation at the electrolyte/lithium interface during charging.

Introduction

The aim of this work was to develop a reliable *in situ* method of investigating potential losses during the cycling of solid-state lithium batteries. This new technology has been the goal of many researchers since the realization by Armand [1] that polymer electrolytes could be applied in this field. Although early studies indicated operating temperatures of about 100 °C would be required [2], recent research has led to the development of polymer electrolytes for room temperature operation [3, 4].

Polymer electrolyte cells are chemically similar to cells with non-aqueous organic liquid electrolytes, e.g., using a solution of lithium triflate in propylene carbonate as the electrolyte and V_6O_{13} as the positive electrode. Although the overall performances are impressive, both capacity losses and limited cycle lives have been observed [5–8] and may be attributed to resistive drops and overpotentials in and between the electrolyte and electrode components. Clearly, the identification of these losses is essential to any logical programme for improving the cell performance. It is known, for example, that mass transport across the interface between lithium and the electrolyte can be impeded by a poorly conducting reaction product between the lithium and the electrolyte constituents; the resistance of such layers have been found to increase with time and cycling, leading to a deterioration of cell performance [9]. On the other hand, the positive electrode may also deteriorate due to structural degradation of the active material or loss of contact with the current collector.

The cells investigated in this work are produced as a thin film laminate of lithium, polymer electrolyte and a composite positive electrode, such that the whole assembly is less than a mm thick. Previous studies of such cells have used complex impedance

*Author to whom correspondence should be addressed.

0378-7753/92/$5.00

[10, 11] and post-cycling cell dissection [12], as well as interpretation of voltage/time curves. However, it is difficult to interpret the latter because of the superposition of contributions from many parts of the cell to give the potential as measured across the terminals.

The use of reference electrode techniques is an obvious way to deconvolute the cell potential into the various components. However, standard reference electrodes cannot be used in this case because the presence of such devices would stand in the current path and interfere with the cycling. This problem was solved here by (i) placing a nickel wire probe of thickness well below that of the electrolyte between two electrolyte layers and, then (ii) plating the wire with lithium from the negative electrode. This enabled both the positive and negative electrode potentials to be monitored with respect to a fixed lithium reference, as well as to each other. Another feature of this work is the use of current interruption to distinguish the slowly relaxing concentration overpotentials from other losses which respond almost immediately to changes in current.

Experimental

Battery construction

Batteries were constructed as layer devices inside an argon atmosphere dry box (water < 5ppm). Materials used in battery construction were as follows: (i) V_6O_{13} composite electrode coated onto nickel foil supplied by Innocell (Denmark); (ii) 'MHB'

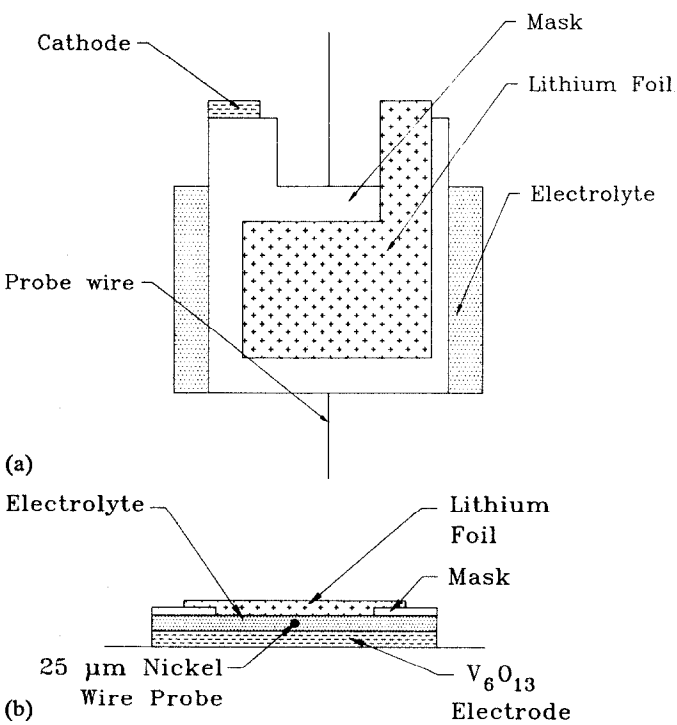

Fig. 1. Thin-layer battery construction incorporating probe wire.

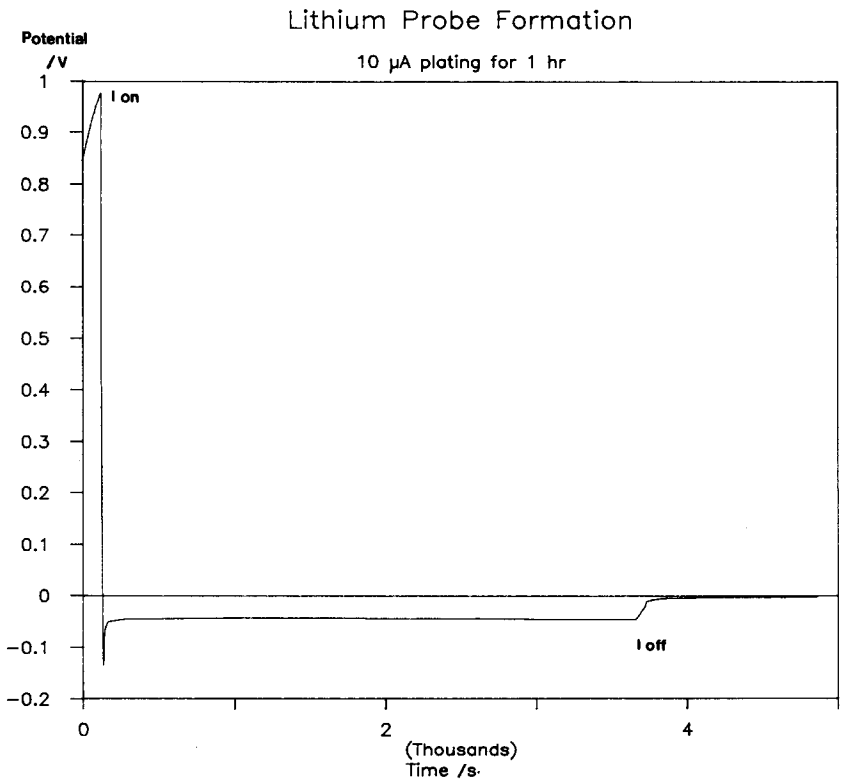

Fig. 2. Reference electrode formation via lithium plating onto nickel wire.

13 electrolyte 100 μm films supplied by Innocell; (iii) 500 μm lithium foil supplied by Lithco (Lithium Corporation Ltd., Cambridge, UK); (iv) 25 μm nickel wire supplied by Goodfellow.

Batteries were constructed as shown in Fig. 1, using the following technique. The positive electrode was attached to a polyethene backing sheet and the first layer of electrolyte film placed over it ensuring that there were no bubbles. The nickel wire was then placed over the electrolyte layer and attached to the backing. A second piece of electrolyte was placed over the wire, again ensuring that there were no bubbles under the film. An acetate mask with a 4 cm^2 window was placed over the electrolyte and a piece of lithium foil was pressed onto the electrolyte. The battery was then sealed with self-adhesive plastic film and the terminal connections made. The battery remained inside the dry box for all of the experiments.

Lithium probe formation

Lithium was plated onto the nickel wire by passing a current of 10 μA between the negative plate of the battery and the probe wire for one hour, whilst monitoring the voltage between the probe wire and the negative plate.

Battery cycling

Batteries were cycled using an in-house produced computer-controlled constant current cycling rig. Batteries were cycled between voltage limits of 3.0 and 1.8 V

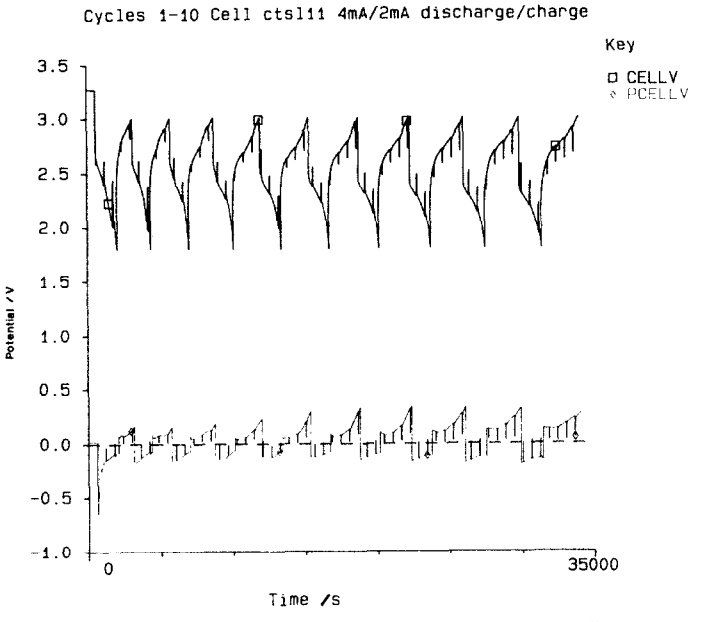

Fig. 3. As-measured cell and probe potentials during cycling.

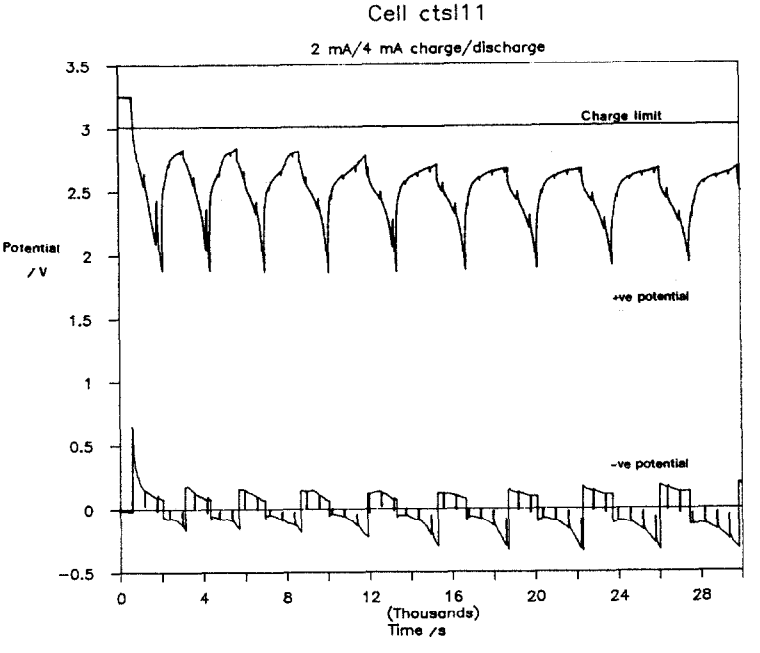

Fig. 4. Deconvolution of data in Fig. 3.

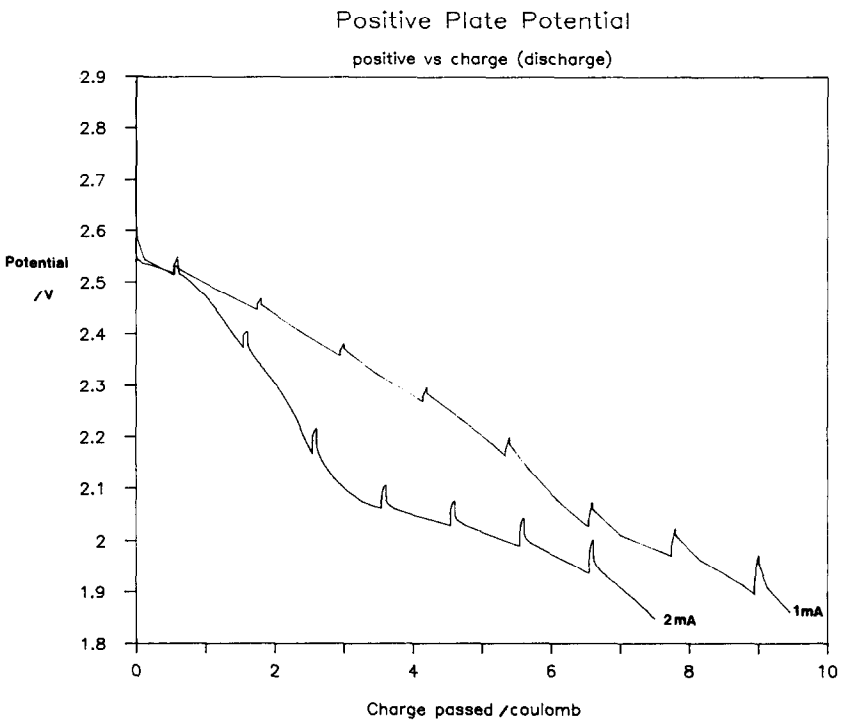

Fig. 5. Positive electrode potential vs. charge (discharge).

(corresponding to a composition of $Li_8V_6O_{13}$) with current interruptions of 30 s applied every 600 s. The cells were cycled at discharge/charge currents of 1.0/0.5, 0.5/0.25 and 0.25/0.125 mA cm^{-2}.

Results and discussion

Lithium probe formation

During the formation of the lithium reference electrode, a lithium plating current is passed onto the thin nickel wire from the relatively-large lithium negative plate. In this case, the current density on the plate is extremely small and the overpotentials can be neglected. The potentials measured on the wire therefore indicate the condition of the wire. At the start of the experiment, the large positive potential is probably due to the presence of nickel oxide on the surface. The initial drop in potential, shown in Fig. 2 shows the gradual reduction of the oxide to nickel and then, as the potential falls well below zero, an overpotential for the nucleation of lithium. After the minimum of -0.15 V, lithium is shown to be formed by a constant potential of -0.057 V which includes and internal resistance (IR) drop. When the current is switched off the reference and negative electrode have the same potential, with the reference remaining stable.

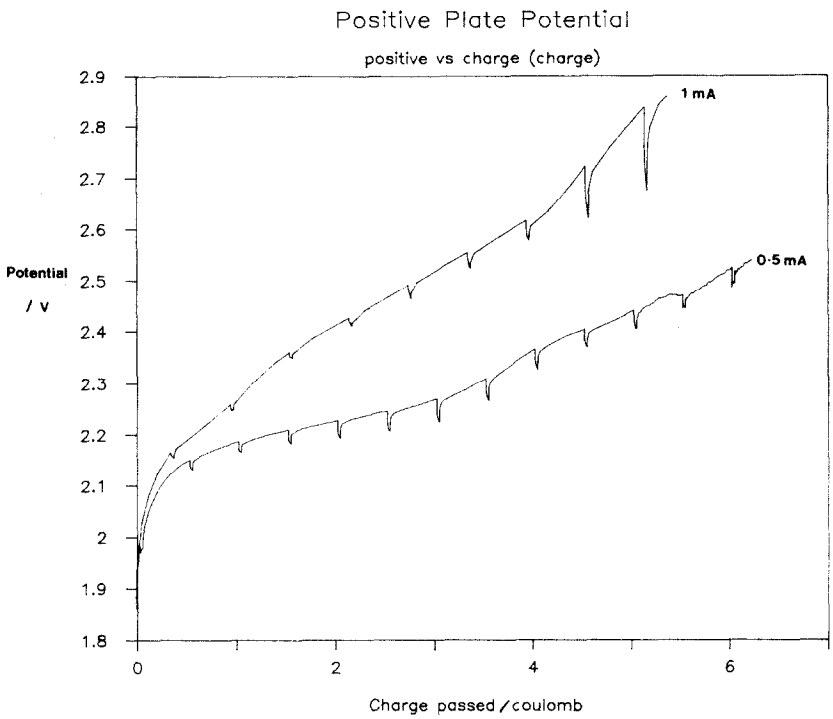

Fig. 6. Positive electrode potential vs. charge (charge).

Deconvolution of electrode potentials

The results for cycles 1 to 10 of cell ctsl11 are shown in Fig. 3. The overall cell potential profiles are similar to those published by other workers [6, 7, 13], and represent the difference $V_{cell} = V_+ - V_-$. Here we also report the probe voltage, $V_{probe} = V_{ref} - V_{-ve}$, where V_{ref} is the potential of the lithium reference electrode which we will take as the zero point for subsequent definition of the single potentials V_+ and V_-. By manipulation of these two sets of results, it is possible to deconvolute the cell voltage into positive and negative electrode contributions:

$$V_{+ve} = V_{cell} - V_{probe} \quad (1)$$

$$V_{-ve} = -V_{probe} \quad (2)$$

The results show that a sharp rise in the negative electrode potential during charge at high current is a major contributor to the cell potential, and causes a premature termination of the charge half-cycle before the positive material is fully charged as shown in Fig. 4.

Positive plate potential

The positive electrode potentials are shown versus charge passed for applied currents of 1 and 2 mA (discharge) and 0.5 and 1 mA (charge) in Figs. 5 and 6. The IR drops are found as the instantaneous change at the end of each current interruption—generally these are 40 mV or less, and correspond to a resistance of only 5 Ω or so. The voltage/charge curves show the expected diffusion overpotential,

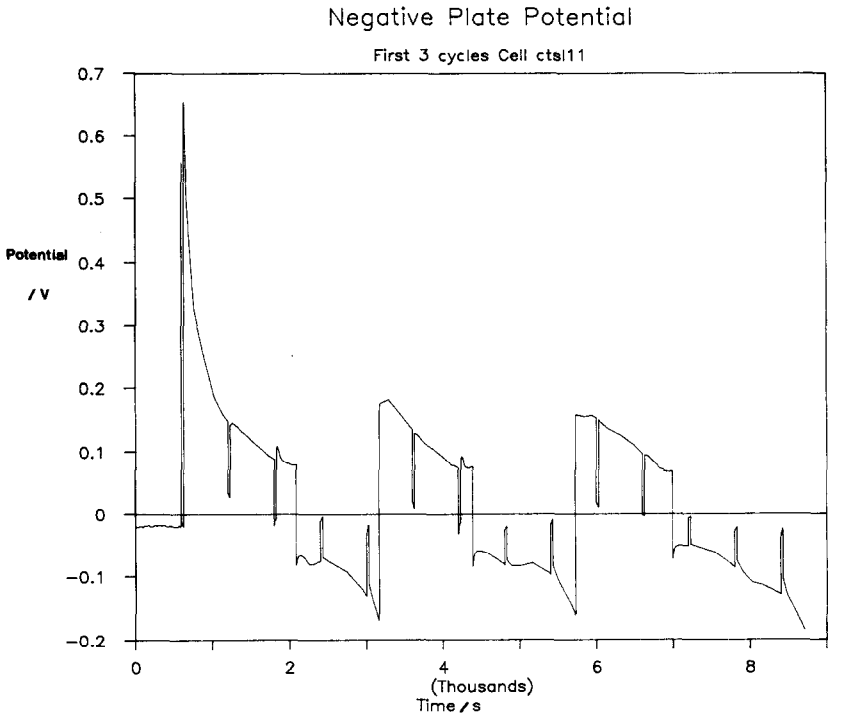

Fig. 7. Negative electrode potential (1 mA cm^{-2} discharge).

indicating an increasing deviation of surface composition from the average composition at increasing current density due to the increasing failure of diffusion to match the rate of lithium insertion demanded. The overpotential is also seen in the relaxations during current interruption, and is roughly proportional to the current.

Negative plate potential

The first feature observed in Fig. 7 is an immediate potential drop of 0.645 V. Taking this as the total ohmic drop between the reference electrode and the lithium surface, at a current of 4 mA, we can calculate a resistance of 161 Ω. This compares well with the total cell resistance as measured by the complex impedance plot of Fig. 8. This suggests that the electrolyte resistance and positive plate resistance are negligible and that the measurement corresponds to a resistive layer between the electrolyte and the lithium. This effect is also shown in Fig. 9 for another cell, where at the time of first current interruption, 600 s into the discharge, the potential had dropped to 0.1 V. This value was maintained for the rest of the discharge cycle and the absence of any residual polarization during current interruption confirms that the voltage loss is purely resistive. On subsequent cycles the initial high resistance is not observed and we assume that the latter was due to a rather compact layer formed on standing at open circuit.

In the first instance of charge, the potential is close to zero and below 50 mV at the first current interruption. However, reference electrode error of up to 50 mV may disguise the true value of the potential here. At the first current interruption a

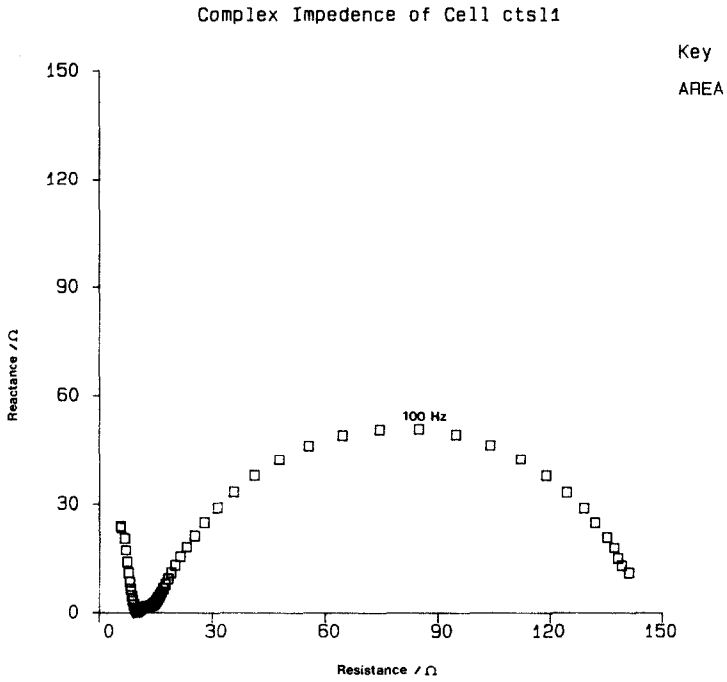

Fig. 8. Complex impedance plot of new cell.

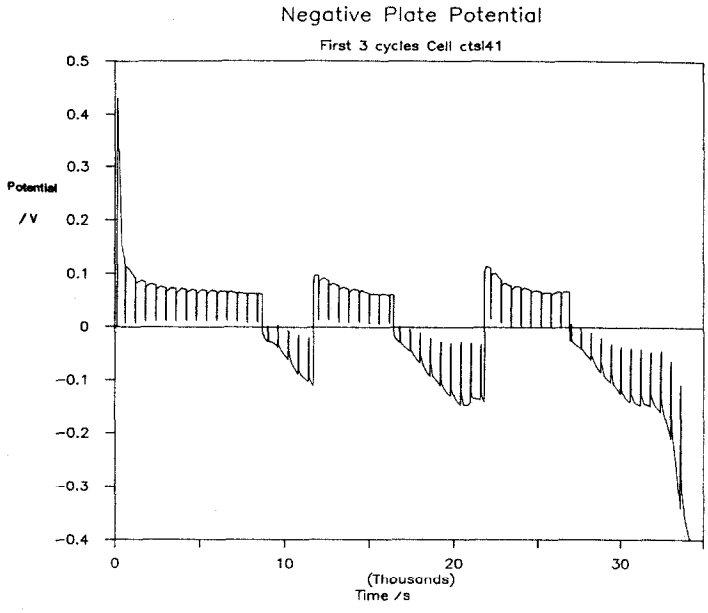

Fig. 9. Negative electrode potential (0.5 mA cm^{-2} discharge).

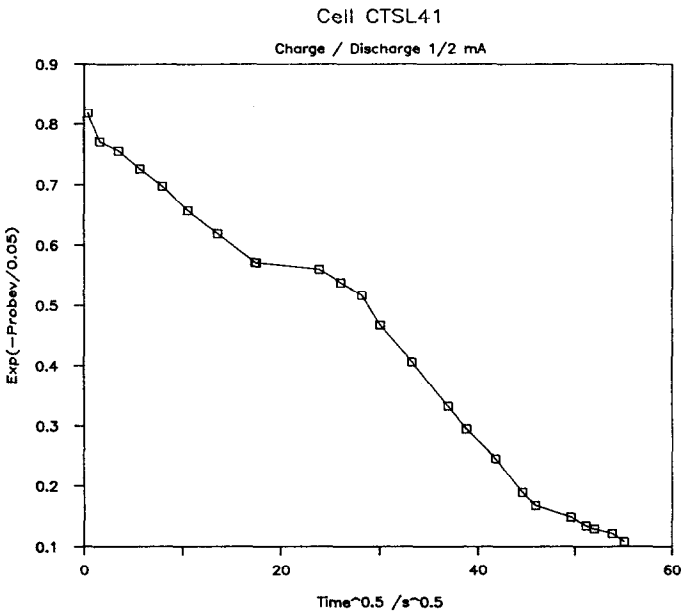

Fig. 10. Plot of $\exp(-\Delta V_{pol}/0.05)$ vs. $t^{1/2}$ for an early charge cycle.

rather small IR drop is registered. Further into the cycle, we observe an increase of both the IR drop and a residual polarization during current interruptions. The increase in the IR drop and the magnitude of the polarization have similar values as predicted by Oldham *et al.* [14] for a model involving depletion of the electroactive ion at the interface in a two-ion system. According to our adaptation of that work, the resistive and polarization losses should each be equal to:

$$\Delta V_{IR} = \Delta V_{pol} = (RT/F) \ln(c/c^\circ) \tag{3}$$

where c and c° are the surface and bulk concentrations respectively of the lithium salt. The total potential measured, while current is flowing, is therefore:

$$\Delta V_{tot} = (2RT/F) \ln(c/c^\circ) = 0.05 \times \ln(c/c^\circ) \text{ at } 25\ ^\circ\text{C}. \tag{4}$$

The surface concentration is given by the solution to the appropriate diffusion equations for constant flux at the surface. In the infinite boundary case, i.e. when the depletion extends only a short distance into a comparatively large region of unstirred electrolyte, the concentration should decrease with the square root of time:

$$c^\circ - c = kt^{1/2} \tag{5}$$

where k is $2i/Fc^\circ \pi^{1/2} D^{1/2}$ [15], i is the current density and D is the lithium ion diffusion coefficient. According to this model a plot of $\exp(-\Delta V_{pol}/0.05)$ versus $t^{1/2}$ should be linear with a gradient of $-k$.

One of the better examples of the above analysis is shown in Fig. 10. The plot was often distorted by the presence of an uncompensated IR drop, leading to an ordinate value of less than 1 at zero time, and finite voltages were noted for times after which the theoretical voltages should have become large enough to terminate the charge half-cycle. However, we can tentatively extract a value of the effective

diffusion coefficient from the slope of the curve. In one example of an almost new cell, this was estimated to be about 10^{-6} cm^2 s^{-1}, assuming a concentration of 0.001 mol cm^{-3}, and a current density equal to the current divided by the total apparent area of the current path. Such a value is lower than that expected for the solvent-plasticized electrolyte, and we interpret the value as an electrolyte diffusion coefficient modified by a tortuosity factor corresponding to the current path through a small volume of electrolyte which has penetrated the layer of reaction product.

Finally, we must interpret the complex impedance plot as the impedance of the composite material at the interface, since the characteristic frequency is too high for the bulk electrolyte. Although it would be theoretically possible to calculate the thickness of the composite layer from the tortuosity factor and the electrolyte conductivity, the turtuosity factor is not considered sufficiently accurate here, therefore that calculation will be deferred until further work can produce more reliable values.

Conclusions

The use of an *in situ* reference electrode has shown to be a powerful technique which reveals the nature of both electrode processes during battery cycling. No interfacial layer effects were found on the positive plate, but the charge process revealed a large overpotential build-up at the negative plate/polymer electrolyte interface. This overpotential is thought to be due to an interfacial layer of a reaction product, penetrated by some electrolyte.

References

1 M. Armand, J. M. Chabagno and M. Duclot, in P. Vashishta, J. N. Mundy and G. K. Shenoy (eds.), *Fast Ion Transport in Solids,* North-Holland, Amsterdam, 1979, p. 13.
2 J. R. Owen, *J. Power Sources, 8* (1981) 88.
3 I. E. Kelly, J. R. Owen and B. C. H. Steele, *J. Power Sources, 14* (1985) 13–21.
4 E. Linden and J. R. Owen, *Solid State Ionics, 28–30* (1988) 994.
5 J. DeSilvestro and O. Haas, *J. Electrochem. Soc., 137* (1) (1990) 5c–22c.
6 B. Scrosati, *Br. Polymer J., 20* (1988) 219–226.
7 M. Z. A. Munshi and B. B. Owens, *Solid State Ionics, 26* (1988) 41–46.
8 A. Hooper, J. S. Lundsgaard and J. R. Owen, *Proc. 3rd Contractors Meet., 1983, Talence, France,* Commission European Communities, EUR 8660 EN53.
9 D. Fauteux, *J. Electrochem. Soc., 135* (1988) 2231–2237.
10 C. C. Hunter, D. C. Sinclair, A. R. West and A. Hooper, *J. Power Sources, 24* (1988) 157–164.
11 P. G. Bruce and F. Krok, *Electrochim. Acta, 33* (1988) 1669–1674.
12 M. Z. A. Munshi and B. B. Owens, *Solid State Ionics, 27* (1988) 251–258.
13 R. Koksbang, I. I. Olsen, P. E. Tonder, N. Knudsen, J. S. Lundsgaard and S. Yde-Andersen, *J. Power Sources, 32* (1990) 175.
14 K. B. Oldham and C. G. Zoski, in C. H. Bamford and R. G. Compton (eds.), *Comprehensive Chemical Kinetics,* Vol. 26, Elsevier, Amsterdam, 1986, pp. 111–119.
15 A. J. Bard and L. Faulkner, *Electrochemical Methods: Fundamentals and Applications,* Wiley-Interscience, New York, 1980, p. 255.